

Supporting Information

Organometallic functionalized non-classical polyoxometalate: synthesis, characterization and electrochemical properties

Panpan Zhang,^a Vikram Singh,^a Jiage Jia,^{a,b} Dongdi Zhang,^{*a} Pengtao Ma,^a Jingping Wang^a and Jingyang Niu^{*a}

^aHenan Key Laboratory of Polyoxometalate Chemistry, College of Chemistry and Chemical Engineering, Henan University, Kaifeng, Henan 475004, P. R. China. E-mail: ddzhang@henu.edu.cn, jyniu@henu.edu.cn; Fax: (+86)-371-23886876

^bState Key Laboratory of Coordination Chemistry, School of Chemistry and Chemical Engineering, Nanjing University, Nanjing 210093, China

CONTENTS

Fig. S1 Summary of polyoxomolybdate-based MCDs.

Table S1 A summary of the factors that affect the synthesis of compounds **1** and **2**.

Fig. S2 Coordination patterns of Te atoms.

Tables S2-3 Selected bond lengths (Å) and angles (°) for **1** and **2**.

Tables S4-5 Bond valence sum calculations for **1** and **2**.

Fig. S3 Charge distribution of oxygen atoms in the polyoxoanion fragments.

Fig. S4 The XRPD patterns of **1** and **2**.

Fig. S5-S8 Electrochemical and electrocatalytic properties of **1** and **2**.

Fig. S9 The IR spectra in the range of 4000–450 cm⁻¹ of **1** and **2**.

Section S1 Thermogravimetric analyses of **1** and **2**.

Section S2 The UV-vis spectra of **1** and **2**.

Section S3 Representation of Compound **2**.

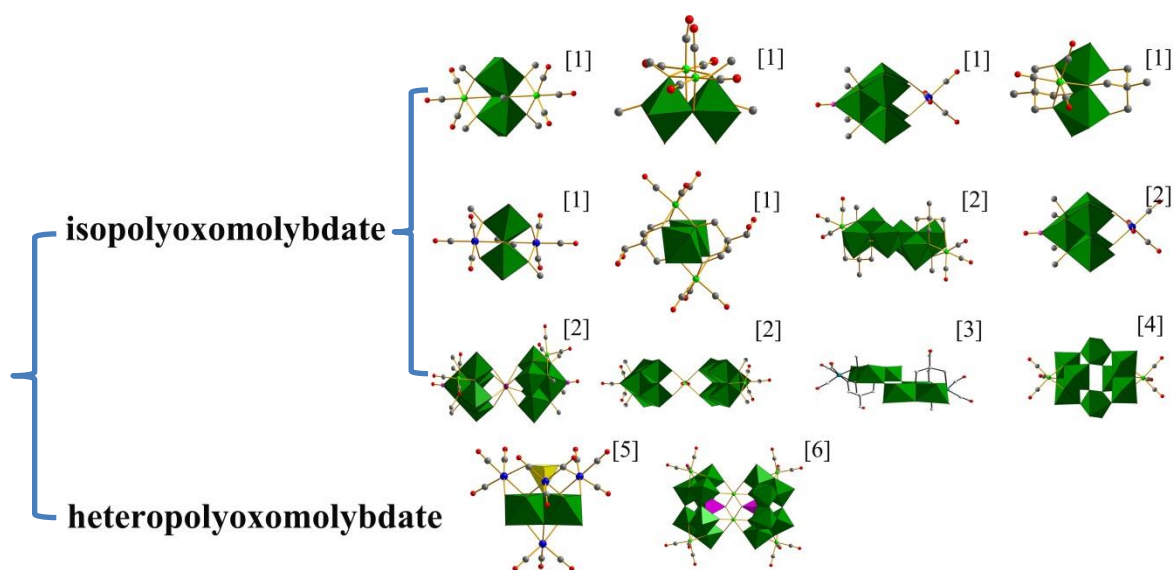


Fig. S1 Summary of polyoxomolybdate-based MCDs.

[1] R. Villanneau, R. Delmont, A. Proust and P. Gouzerh, *Chem. Weinh. Bergstr. Ger.*, 2000, **6**, 1184–1192.

[2] R. Villanneau, A. Proust, F. Robert and P. Gouzerh, *Chem. Eur. J.*, 2003, **9**, 1982–1990.

[3] W. Wang, J. Li, J. Niu, *Chem. Res. Chinese. Universities.*, 2008, **24(6)**, 675–678.

[4] D. Zhang, J. Zhao, Y. Zhang, X. Hu, L. Li, P. Ma, J. Wang and J. Niu, *Dalton Trans.*, 2013, **42**, 2696–2699.

[5] Z. Huo, J. Guo, J. Lu, Q. Xu, P. Ma, J. Zhao, D. Zhang, J. Niu and J. Wang, *RSC Adv.*, 2015, **5**, 69006–69009.

[6] V. Singh, Y. Zhang, L. Yang, P. Ma, D. Zhang, C. Zhang, L. Yu, J. Niu and J. Wang, *Molecules.*, 2017, **22**, 1351–1365.

Table S1 A summary of the factors that affect the synthesis of compounds **1** and **2**. ("√" : work; "×" :do not work)

Factors	Conditions		Results
	1	2	
pH	< 4.8	< 5.1	×
	4.8 – 5.2	5.1 – 5.3	√
	> 5.2	> 5.3	×
molar ratios of solution	3:10, 3:12, 3:14, 3:16	3:8, 3:12, 3:14, 3:16	×
	3:8	3:10	√
material ratios (Mo ₇ : Na ₂ TeO ₃)	> 1:1	> 5:1	×
	1:1	5:1	√
	< 1:1	< 5:1	×
temperature	< 70 °C		×
	70 °C – 80 °C		√
	> 80 °C		×
countercation	Ammonium chloride, Tetramethylammonium chloride		√
	chloride, lithium, sodium, potassium chloride, tetrabutylammounium bromide,		×
	guanidine hydrochloride		×

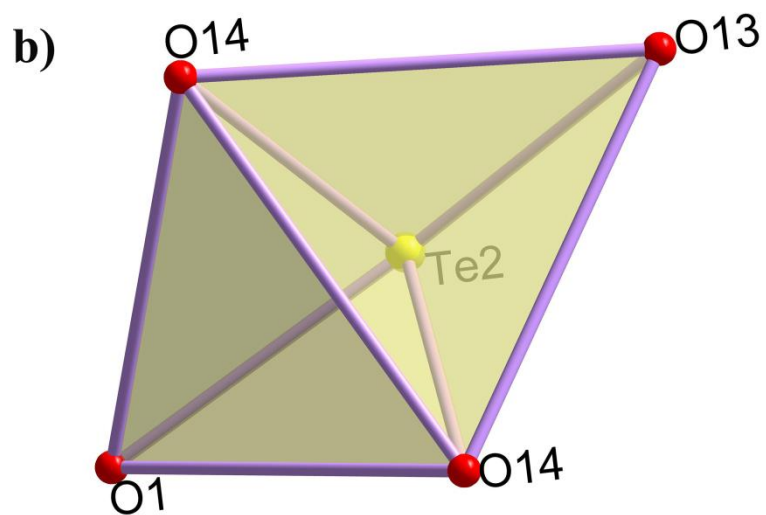
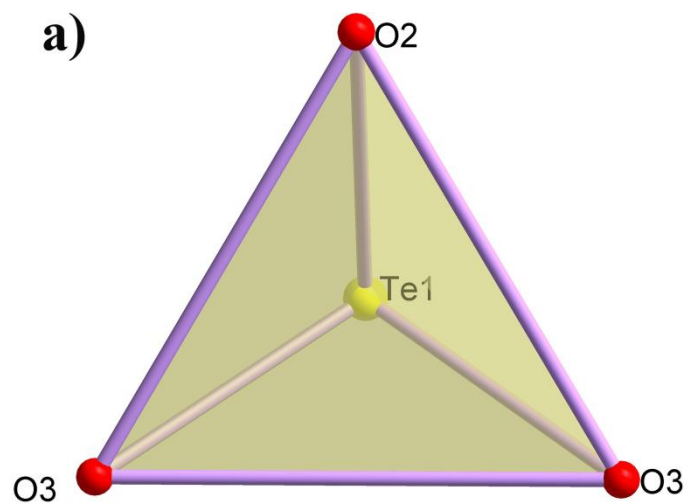


Fig. S2 Coordination patterns of Te atoms. a) Polyhedral representation of Te 1 atom; b) Polyhedral representations of Te 2 atom. Color code: Te, yellow balls; O, red balls.

Table S2 Selected bond lengths (Å) for **1** and **2**

1		2	
Bond	Length	Bond	Length
Te1-O2	1.941(3)	Te1-O2	1.924(4)
Te1-O3'	1.867(2)	Te1-O5	1.871(3)
Te1-O3	1.867(2)	Te1-O5'	1.871(3)
Te2-O1	2.142(3)	Te2-O1	1.980(5)
Te2-O13	1.996(3)	Te2-O3	1.906(4)
Te2-O14'	1.901(2)	Te2-O3'	1.906(4)
Te2-O14	1.901(2)	Te2-O7	2.146(5)
Mn1-O6	2.091(4)	Re1-O4	2.120(4)
Mn1-O7	2.033(3)	Re1-O4'	2.120(4)
Mn1-O7'	2.033(3)	Re1-O10	2.194(6)
Mn1-C1	1.796(5)	Re1-C1	1.883(6)
Mn1-C1'	1.796(5)	Re1-C1'	1.883(6)
Mn1-C2	1.792(7)	Re1-C2	1.832(8)
C1-O27	1.145(6)	C1-O27	1.184(8)
C1-O27'	1.145(6)	C1-O27'	1.184(8)
C2-O28	1.131(8)	C1-O28	1.223(11)

Table S3 Selected Bond Angles (°) for **1** and **2**.

1		2	
Bond	Angle	Bond	Angle
O3-Te1-O2	94.41(10)	O5-Te1-O2	94.54(14)
O3'-Te1-O2	94.41(10)	O5'-Te1-O2	94.54(14)
O3-Te1-O3'	95.77(15)	O5-Te1-O5'	95.9(2)
O13-Te2-O1	165.11(13)	O1-Te2-O7	165.21(19)
O14-Te2-O1	77.42(10)	O3'-Te2-O1	93.06(14)
O14'-Te2-O1	77.42(10)	O3-Te2-O1	93.06(14)
O14'-Te2-O13	93.00(10)	O3'-Te2-O3	98.5(2)
O14-Te2-O13	93.01(10)	O3'-Te2-O7	77.43(13)
O14'-Te2-O14	98.47(15)	O3-Te2-O7	77.43(13)

Table S4 BVS of Te and Mo atoms of compounds **1** and **2**.

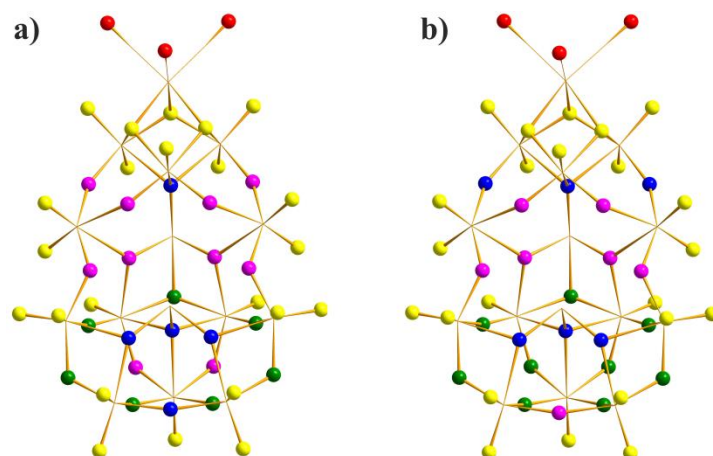
1		2	
Atoms	BVS for Mo, Te	Atoms	BVS for Mo, Te
Te1	3.79	Te1	3.81
Te2	4.04	Te2	4.04
Mo1	6.14	Mo1	6.13
Mo2	6.02	Mo2	5.93
Mo3	6.16	Mo3	6.06
Mo4	6.07	Mo4	6.10
Mo5	5.81	Mo5	6.02
Mo6	6.05	Mo6	6.06
Mo7	6.11	Mo7	6.06

Table S5 BVS of O atoms of compounds **1** and **2**.

1		2	
Atoms	BVS	Atoms	BVS
O1	1.88	O1	2.01
O2	2.06	O2	2.06
O3	2.15	O3	1.94
O4	1.77	O4	1.09
O5	1.99	O5	2.13
O6	1.65	O6	1.85
O7	1.03	O7	1.86
O8	1.86	O8	1.84
O9	1.99	O9	1.91
O10	1.68	O10	1.51
O11	1.88	O11	1.66
O12	1.89	O12	1.71
O13	2.01	O13	2.21
O14	1.98	O14	1.87
O15	1.69	O15	1.95
O16	1.66	O16	1.90
O17	1.92	O17	1.67
O18	1.87	O18	1.77
O19	2.01	O19	1.71
O20	1.73	O20	1.69
O21	1.74	O21	1.72
O22	1.70	O22	1.72

O23	1.69	O23	1.99
O24	1.76	O24	1.71
O25	1.71	O25	1.63
O26	1.73	O26	1.72

The red fonts represent Monoprotonation oxygen atoms.








Oxygen atom	Bond valence sum range	Number in 1	Number in 2
	1.03 – 1.77	21	23
	1.84 – 1.89	7	9
	1.90 – 1.99	10	7
	2.01 – 2.21	5	6
	O atoms in carbonyl fragment		

Fig. S3 Charge distribution of oxygen atoms in the polyoxoanion fragment of **1** and **2**. Oxygen atoms with different bond valence sums are represented by different colours.

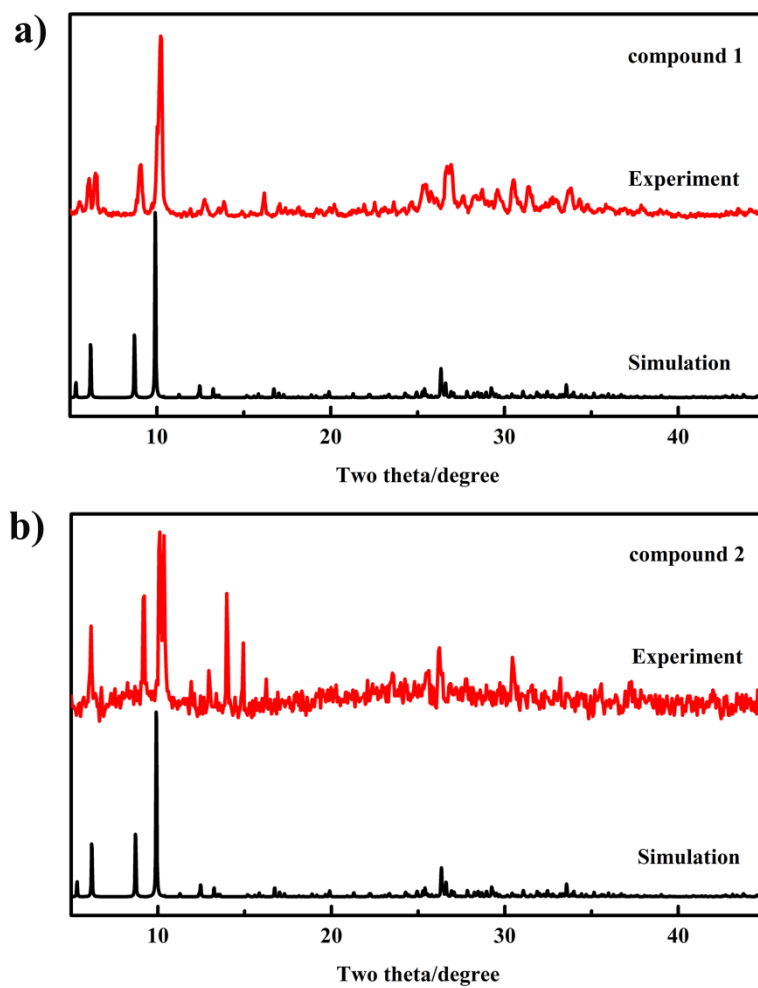


Fig. S4 a) XRD patterns of compound **1** (red), simulation XRD patterns of **1** (black). b) XRD patterns of compound **2** (red), simulation XRD patterns of **2** (black).

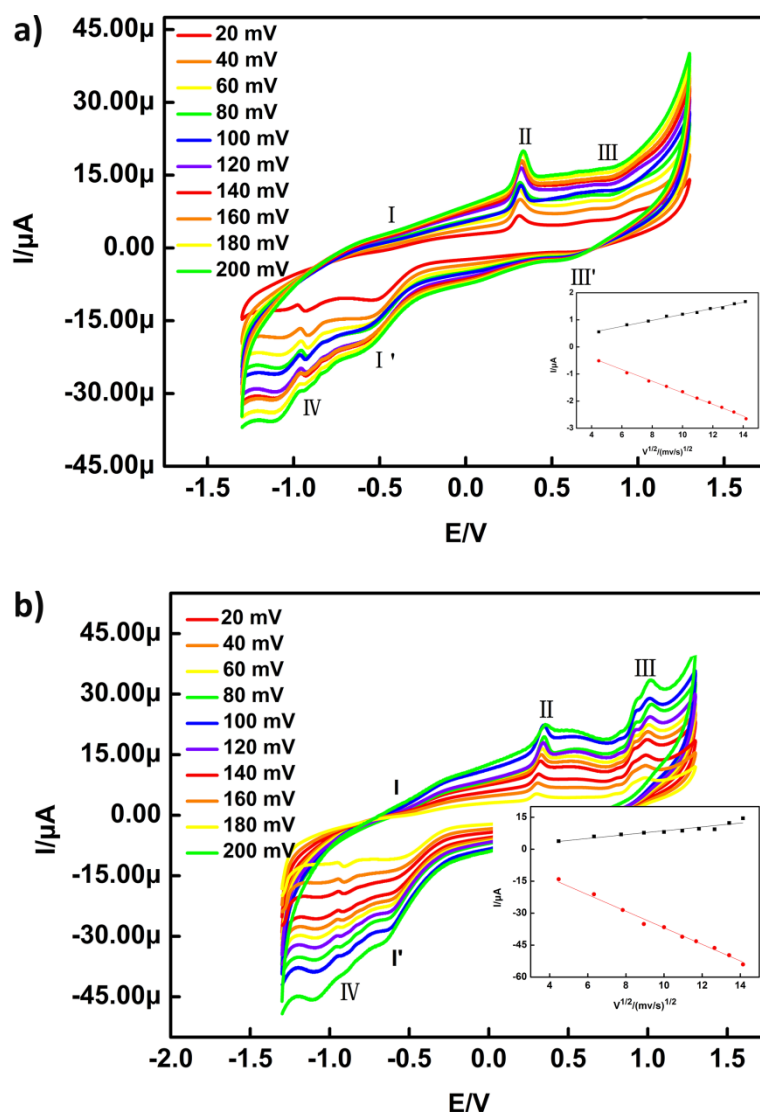


Fig. S5 (a) Cyclic voltammograms of **1** at different scan rate (from 20 mV s^{-1} to 200 mV s^{-1}). Inset plot the variation of the peak current intensity for the Mo is proportional to the the the square root plot of the scan rates from 20 to 200 mV s^{-1} ; (b) Cyclic voltammograms of **2** at different scan rate (from 20 mV s^{-1} to 200 mV s^{-1}). Inset plot the variation of the peak current intensity for the Mo is proportional to the the square root plot of the scan rates from 20 to 200 mV s^{-1} .

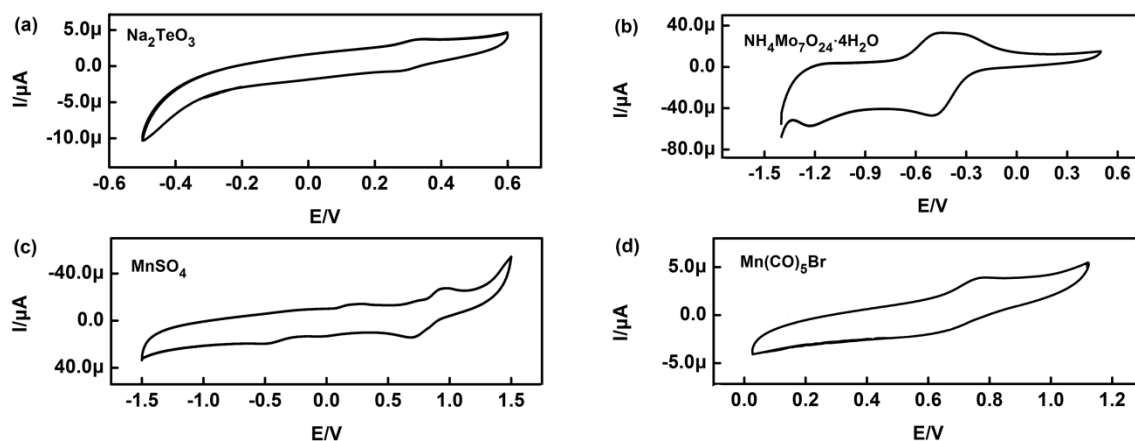


Fig. S6 (a) Cyclic voltammograms of the Na_2TeO_3 at the scan rates of 100 mV s^{-1} ; (b) Cyclic voltammograms of the $\text{NH}_4\text{Mo}_7\text{O}_{24}\cdot 4\text{H}_2\text{O}$ at the scan rates of 100 mV s^{-1} ; (c) Cyclic voltammograms of the MnSO_4 at the scan rates of 100 mV s^{-1} ; (d) Cyclic voltammograms of the $\text{Mn}(\text{CO})_5\text{Br}$ at the scan rates of 100 mV s^{-1} .

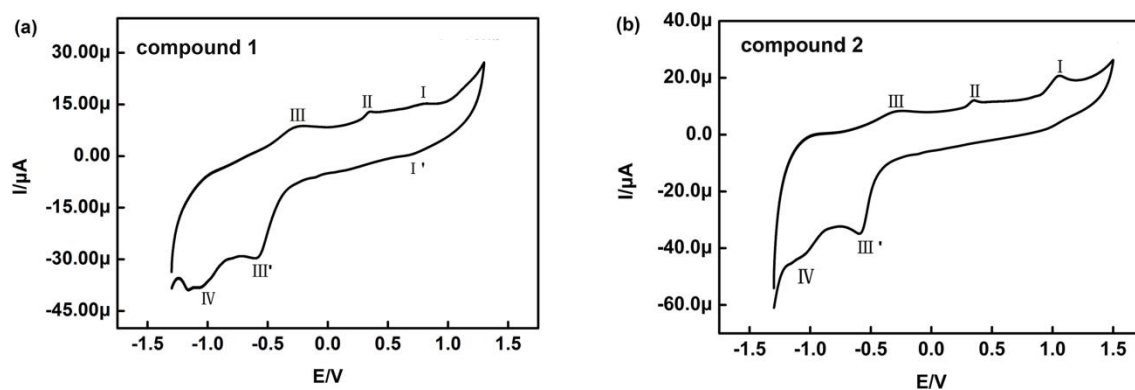


Fig. S7 a) Voltammetric curve of **1** at 100 mV s^{-1} ; b) Voltammetric curve of **2** at 100 mV s^{-1} .

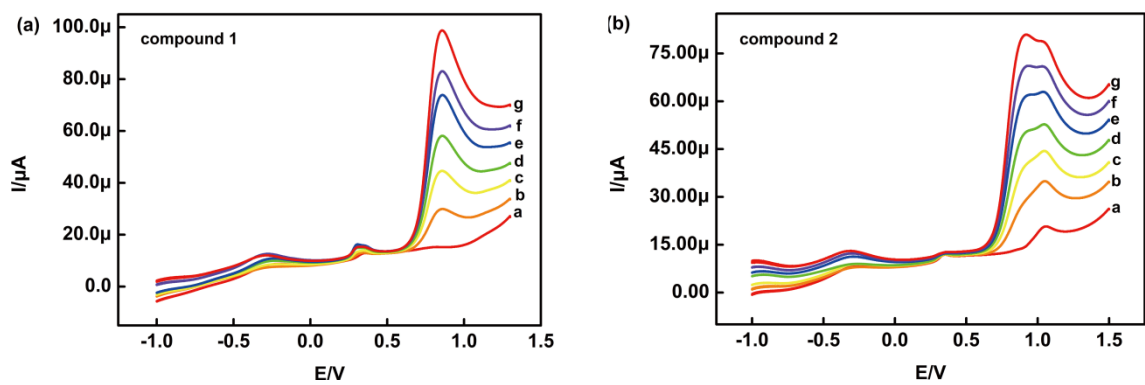


Fig. S8 a) Voltammetric response of electrocatalytic nitrite of **1**; b) Voltammetric response of electrocatalytic nitrite of **2**.

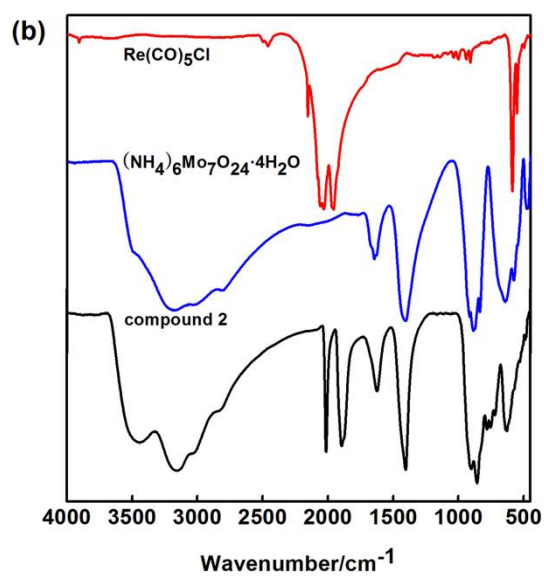
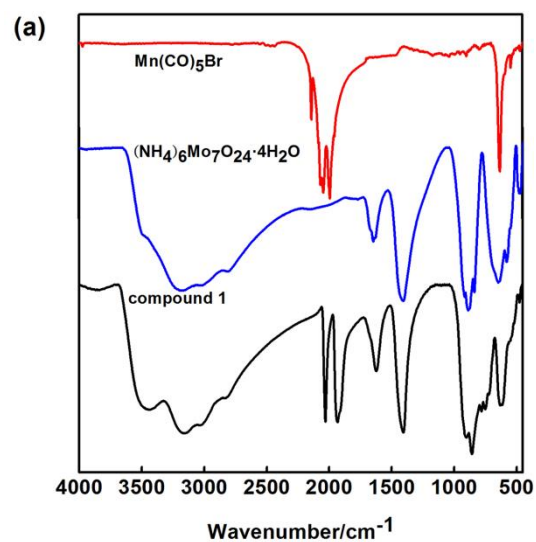


Fig. S9 IR spectra for Mn(CO)₅Br, **1** and (NH₄)₆Mo₇O₂₄·4H₂O (middle) and **2** Re(CO)₅Cl (top) in the region between 4000 to 450 cm⁻¹

Section S1 Thermogravimetric analyses of **1** and **2**.

To examine the thermal stability of compounds **1** and **2**, TG analyses were carried out under a N₂ atmosphere with a heating rate of 10 °C min⁻¹ in the temperature range of 30–630 °C and 30–700 °C for the two compounds, respectively (Fig. S7). Both compounds show a distinct weight-loss process. The TG curve of **1** exhibits two continuous weight loss stages below 500 °C corresponding to the release of twenty one water molecules (protons were in the form of water), five ammonium cations, three carbonyl units, and the sublimation of two TeO₂, giving a total loss of 23.90% (calcd 24.24%) (Fig. S10a). The TG curve of **2** can be regarded as successive two-step weightlessness, giving a total loss of 32.75% in the range of 30–700°C. The first stage from 30–300°C is assigned to the loss of eight ammonium cations and six lattice water molecules, and the observed weight loss 8.93% is consistent with the calculated value 8.37%. The second stage with the weight loss of 23.82% may be attributed to the removal of three carbonyl units, seven water molecules (one of the protons is in the form of water), the sublimation of two TeO₂ and ten O₂ (may be due to the collapse of the polyacid skeleton)(calcd 23.12%) (Fig. S10b).

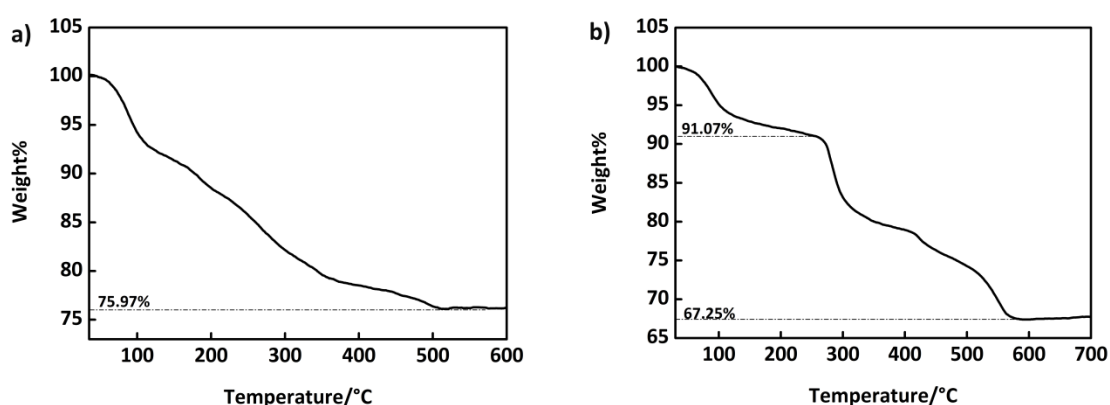


Fig. S10 a) The TG curve of **1**; b) The TG curve of **2**

Section S2 The UV-vis spectra of **1** and **2**.

The UV-Vis absorption spectrum of compounds **1** and **2** are investigated in the aqueous solution. The clusters show similar characteristic electronic absorption bands, the higher energy bands at ca. 215 nm can be assigned to Ot \rightarrow Mo charge transfer transitions,¹ while, the absorption bands at ca. 358 nm can be attributed to Mn (π) \rightarrow CO (π^*) transition which is not obvious resulting from the lower concentration,² indicating the presence of manganese carbonyl unit. In order to investigate the stability of **1** and **2**, the UV-Vis spectra are recorded in the regular intervals for 7 h in the aqueous solution. The time variable UV-Vis spectra manifest that compound **1** and **2** remain stable for at least 7 h at room temperature (Fig. S11-S12). As we all know, POMs stability and formation are pH dependent, and thus further scientific studies of in-situ UV-Vis spectra at different pH values in the aforementioned solvent are also undertaken. With the increase in pH beyond 4.18, the absorption band at ca. 215 nm show slightly red shift, with higher molar absorption coefficient (Fig. S13a). Such variations in electronic absorption features might imply a stepwise decomposition process of polyoxoanions. When adjust to pH lower than 4.18, the absorption band appears blue shifted, in the meantime the absorption become apparently stronger, along with a weak absorption band at ca. 220 nm, which derive from the POMs skeleton of the gradual collapse (Fig. S13a). Conclusively, compounds **1** and **2** are unstable at pH higher or lower 4.18 (Fig. S12—S14).

1 S. Bassil, S. Nellutla, U. Kortz, A. C. Stowe, J. van Tol, N. S. Dalal, B. Keita and L. Nadjo, *Inorg. Chem.*, 2005, **44**, 2659–2665.

2 (a) D. Burdinski, E. Bothe and K. Wieghardt, *Inorg. Chem.*, 2000, **39**, 105–116. (b) M. Busby, P. Matousek, M. Towrie, I. P. Clark, M. Motevalli, F. Hartl and A. Vlček, *Inorg. Chem.*, 2004, **43**, 4523–4530. (c) H. D. Batey, A. C. Whitwood and A. K. Duhme-Klair, *Inorg. Chem.*, 2007, **46**, 6516–6528.

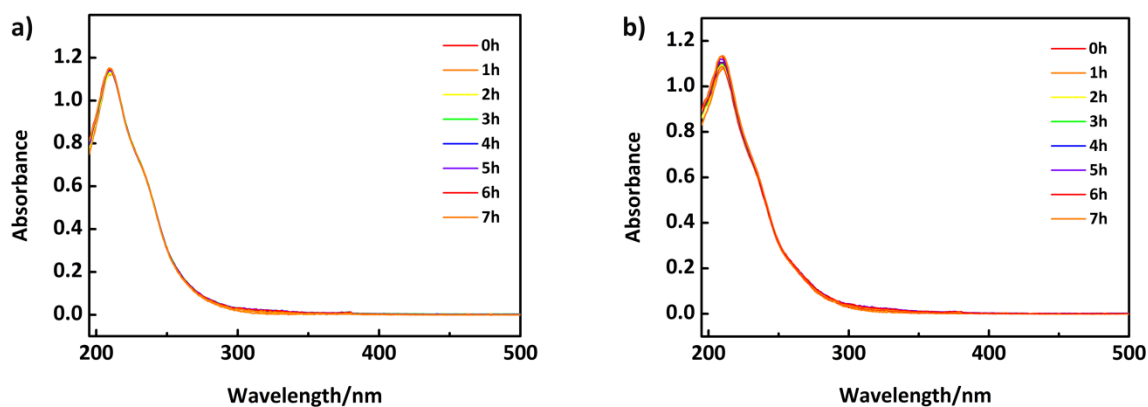


Fig. S11 The aging of the solution of **1** (left), **2** (right) detected by the in-situ UV-Vis spectra.

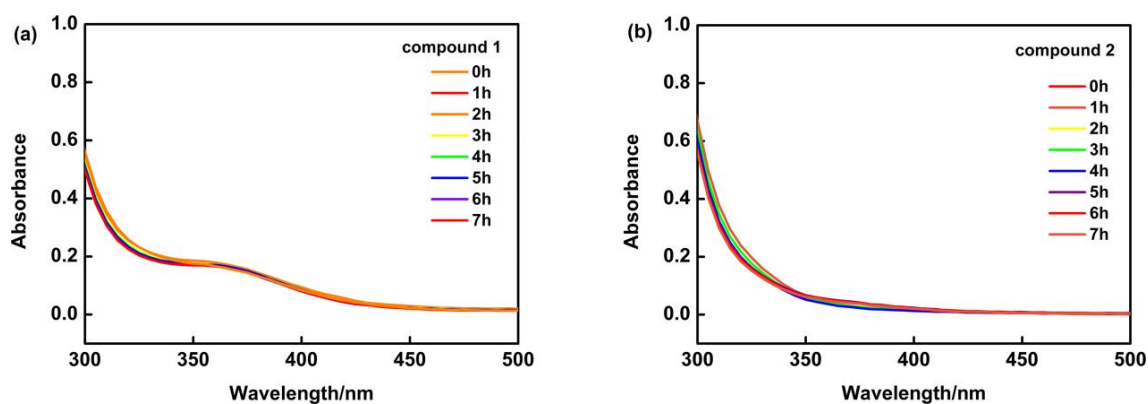


Fig. S12 (a) the carbonyl manganese UV-Vis spectra evolution of **1** in the aqueous; (b) the carbonyl rhenium UV-Vis spectral evolution of **2** in the aqueous.

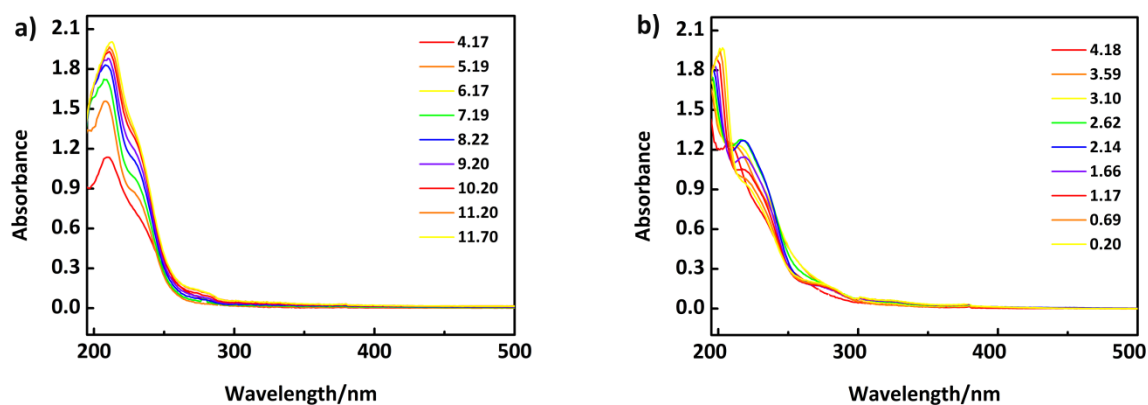


Fig. S13 (a) The UV-Vis spectra evolution of **1** in the alkaline direction; (b) The UV-Vis spectral evolution of **1** in the acidic direction.

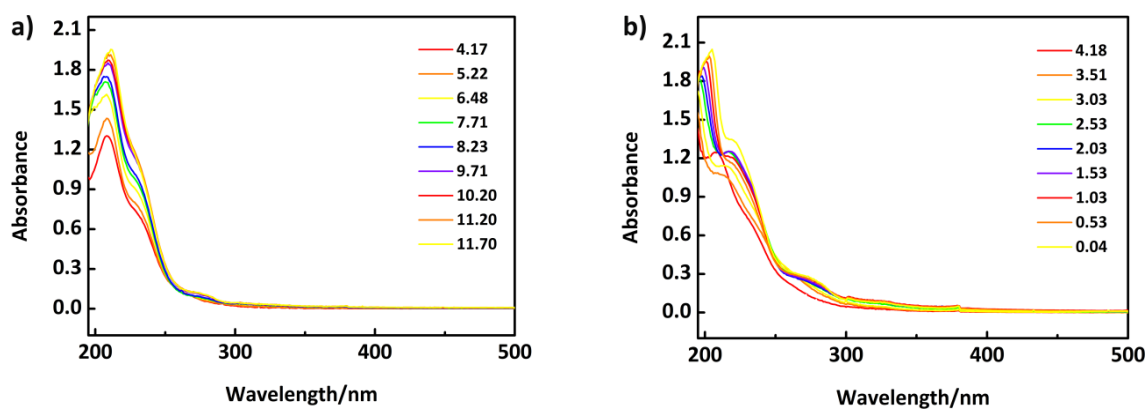


Fig. S14 (a) the UV-Vis spectra evolution of **2** in the alkaline direction; (b) The UV-Vis spectral evolution of **2** in the acidic direction.

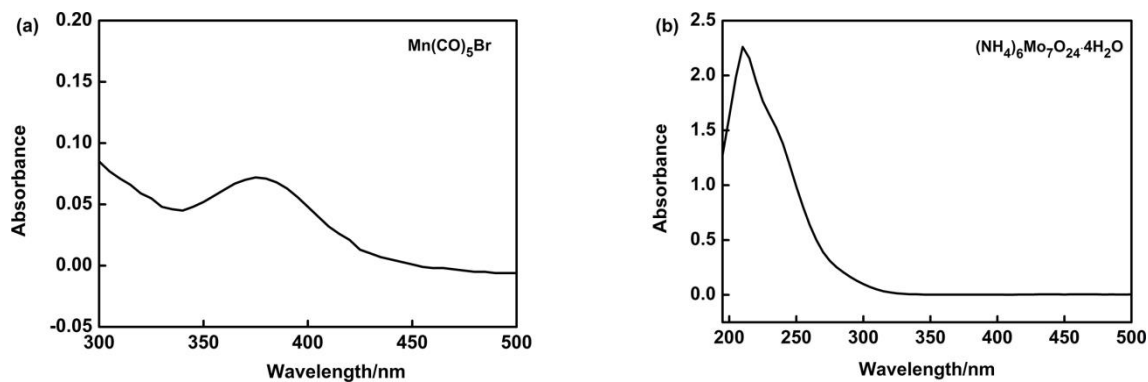


Fig. S15 (a) The UV-Vis spectra of the raw material $\text{Mn}(\text{CO})_5\text{Br}$; (b) The UV-Vis spectra of the raw material $(\text{NH}_4)_6\text{Mo}_7\text{O}_{24}$.

Section S3 Representation of compound 2.

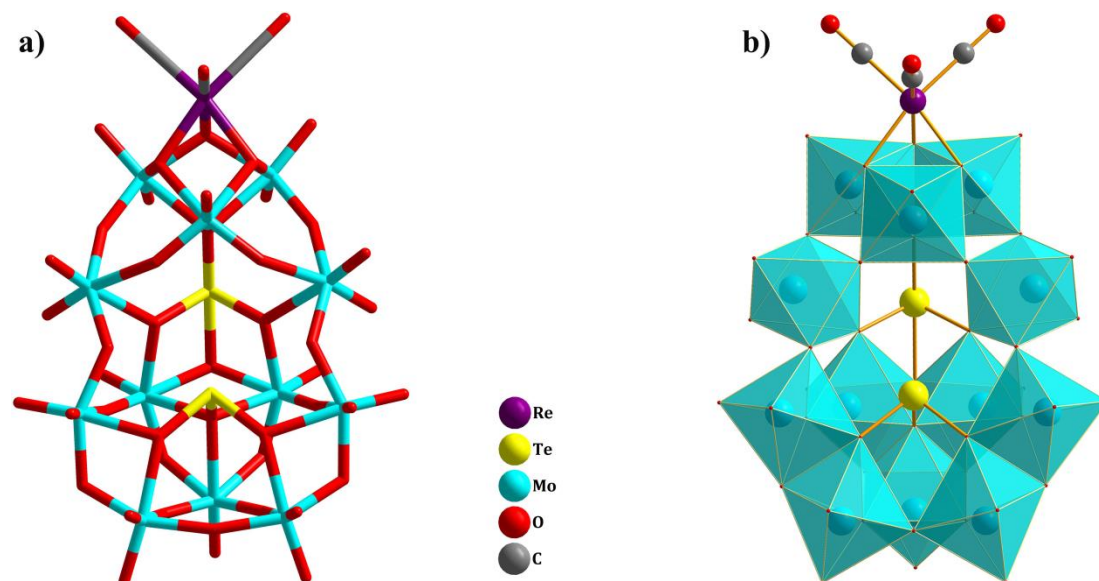


Fig. S16 a) Ball-and-stick representation of **2**; b) Polyhedral and ball-and-stick representations of $[\text{Te}_2\text{Mo}_{12}(\text{OH})\text{O}_{44}][\text{Re}(\text{CO})_3]^{8-}$. Color code: Te, wine red balls; Mo, azure balls; Re, wine red ball; O, red balls; C, grey balls; MoO_6 octahedra, azure. Water molecules and cations are omitted for clarity.